The Catalytic Pathway of Cytochrome P450cam at Atomic Resolution

Ilme Schlichting,[1]* Joel Berendzen,[2] Kelvin Chu,[2]† Ann M. Stock,[3] Shelley A. Maves,[4] David E. Benson,[4] Robert M. Sweet,[5] Dagmar Ringe,[6] Gregory A. Petsko,[6] Stephen G. Sligar[1,4]

Members of the cytochrome P450 superfamily catalyze the addition of molecular oxygen to nonactivated hydrocarbons at physiological temperature—a reaction that requires high temperature to proceed in the absence of a catalyst. Structures were obtained for three intermediates in the hydroxylation reaction of camphor by P450cam with trapping techniques and cryocrystallography. The structure of the ferrous dioxygen adduct of P450cam was determined with 0.91 angstrom wavelength x-rays; irradiation with 1.5 angstrom x-rays results in breakdown of the dioxygen molecule to an intermediate that would be consistent with an oxyferryl species. The structures show conformational changes in several important residues and reveal a network of bound water molecules that may provide the protons needed for the reaction.

Cytochrome P450 enzymes are ubiquitous heme-containing monooxygenases named for the absorption band at 450 nm of their carbon monoxide (CO) form (*1*). They are involved in a number of vital processes including carcinogenesis and drug metabolism as well as the biosynthesis of steroids or lipids and the degradation of xenobiotics (*2*), making them potentially useful in, e.g., bioremediation or synthesis. They are the biological equivalent of a blowtorch: P450 enzymes catalyze the stereospecific hydroxylation of nonactivated hydrocarbons at physiological temperature—a reaction that, uncatalyzed, requires extremely high temperatures to proceed, even nonspecifically. The mechanism by which these enzymes are able to activate oxygen to carry out this difficult chemistry has long been investigated, but many details have not yet been established. In particular, the mechanism of activation of the bound oxygen molecule and the nature of the activated oxygen species remain uncertain.

Structurally and biochemically, the best characterized P450 is P450cam (*3*), which catalyzes the regio- and stereospecific hydroxylation of camphor to 5-*exo*-hydroxycamphor according to the mechanism shown in Fig. 1. P450cam was the first member of the P450 superfamily whose three-dimensional structure was determined, and both the binary enzyme-substrate (**2**; throughout the text, the bold numbers refer to species in Fig. 1) and enzyme-product (**4**) complexes have been so characterized (*4*). Some features of the dioxygen-bound or activated oxygen intermediates, in particular the geometry of the six-coordinate low-spin heme, have been deduced from the structure of the ferrous (Fe^{II+}) carbonmonoxy complex (**3**) of P450cam (*5*). However, the binding of carbon monoxide to heme is likely to be different in a number of important ways from the binding of oxygen (*6*), and regardless, carbon monoxide is an inhibitor, not a substrate, of P450cam. Hence, the primary evidence for the structures of the ferrous enzyme-substrate complex (**5**), the dioxy intermediate (**6**), and the mysterious "activated oxygen" species (**7**) that actually carries out the hydroxylation derives from spectroscopic studies of various P450s and model compounds (*7*) and from analogy with other heme proteins such as peroxidases (*8*).

The crystal structure of the oxygenated (dioxy) intermediate (**6**) could not be determined previously because it decays with a half-life of 10 min at 4°C in solution through autooxidation (*9*). Similar obstacles have prevented direct observation of the remaining intermediates (**5** and **7**) by x-ray diffraction.

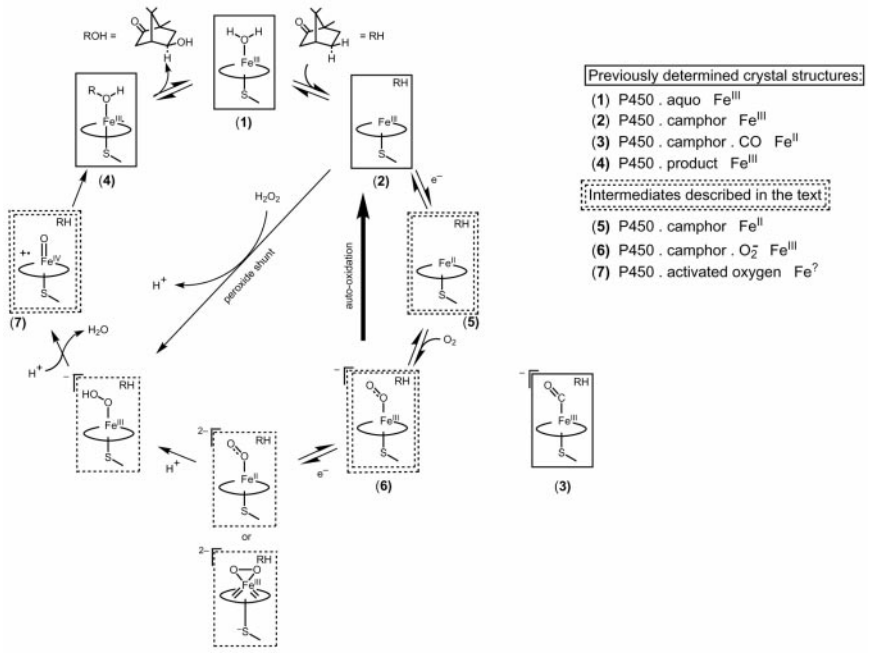

Fig. 1. Reaction pathway of P450cam. The catalytic cycle of *Pseudomonas putida* P450cam consists of reversible substrate binding, which converts the six-coordinate, low-spin met form [**1** (*4*)] of the protein to the five-coordinate, high-spin Fe^{III} camphor complex [**2** (*4*)]; addition of the first electron, which reduces the enzyme to the five-coordinate Fe^{II} camphor complex (**5**); binding of molecular oxygen to give the six-coordinate Fe^{II}-O_2 dioxygen intermediate (**6**); addition of a second electron and two protons followed by cleavage of the oxygen-oxygen bond to produce a molecule of water and an oxidizing species, the so-called activated oxygen intermediate (**7**); and insertion of the iron-bound oxygen into the substrate to produce 5-*exo*-hydroxycamphor [**4** (*4*)] and product release. The unnumbered oxygen species shown in dotted boxes between **6** and **7** represent other possible species along the reaction pathway. Also shown is the previously determined complex of P450.camphor.CO (*6*).

[1]Max Planck Institute for Molecular Physiology, Department of Physical Biochemistry, Otto Hahn Strasse 11, 44227 Dortmund, Germany. [2]Biophysics Group, Mail Stop D454, Los Alamos National Laboratory, Los Alamos, NM 87545, USA. [3]Center for Advanced Biotechnology and Medicine, 679 Joes Lane, Piscataway, NJ 08854–5638, USA. [4]Beckman Institute, University of Illinois, 405 N. Mathews, Urbana, IL 61801, USA. [5]Biology Department, Brookhaven National Laboratory, Upton, NY 11973, USA. [6]Rosenstiel Center, Brandeis University, 415 South Street, Waltham, MA 02254–9110, USA.

*To whom correspondence should be addressed. E-mail: ilme.schlichting@mpi-dortmund.mpg.de

†Present address: Department of Physics, Cook Building, University of Vermont, Burlington, VT 05405–0125, USA.

To obtain a better understanding of the structural basis of the enormous catalytic power of P450 enzymes, we set out to determine the crystal structures of the metastable species on the P450cam reaction pathway.

Recent developments in the use of cryogenic temperatures and rapid data-collection techniques in protein crystallography have opened up the possibility of direct structural characterization of normally unstable intermediates in enzyme-catalyzed reactions (*10*). The major roadblocks in trapping such intermediates are initiating reactions simultaneously in protein crystals (*11*) and avoiding the buildup of mixtures as the reaction proceeds (*12*). But if conditions can be found for a crystalline enzyme under which intermediates could be generated rapidly and accumulated to high occupancy, it would be possible to obtain a set of "time-lapse" pictures, at atomic resolution, of the transformation from substrate to product. Such conditions have now been found for the reaction catalyzed by cytochrome P450cam from *Pseudomonas putida*. The structures obtained are consistent with the results of other techniques such as spectroscopy and thus enable specific chemical structures to be assigned to these intermediates. Taken together, they also provide a model for the proton transfer steps of the reaction and suggest a role for the highly conserved and catalytically crucial Asp^{251}.

Structure determination of unstable complexes of P450cam: Experimental strategy. There are a number of technical challenges to the determination of the structures of short-lived intermediates in a catalytic cycle. One of these, simultaneous initiation of the reaction throughout the crystal, is minimized by the ordered mechanism of P450cam (Fig. 1): Most of the intermediates accumulate until provided with a specific trigger (addition of electron or oxygen) for further conversion. Another challenge is the relatively short lifetimes of most enzyme intermediates relative to the time normally required to collect an x-ray data set. Diffraction data for unstable species can be collected rapidly either by polychromatic (Laue) or fast monochromatic diffraction techniques (*13*). The former—and in most cases, the latter—requires the use of synchrotron radiation and often that the reaction be slowed, e.g., by mutagenesis or low temperature (*14*). Because the Laue approach was not applicable in our case (see below), we freeze-trapped the various complexes of P450cam and determined their structures using monochromatic x-rays.

Crystallographic observation of the activated oxygen intermediate of P450cam would seem to be prohibited by a unique feature of its stepwise two-electron redox reaction: Although the first electron can be supplied by a variety of convenient sources such as dithionite, efficient donation of the second electron both in vivo and in vitro comes from another protein, putidaredoxin (*15*). Putidaredoxin is not present in P450cam crystals and cannot be diffused into the lattice. We overcame this problem by exploiting a different source of electrons. Reduction of metallo-proteins by electrons produced by x-ray radiolysis of water has been observed in other systems (*16*) and has been used deliberately in electron paramagnetic resonance experiments on P450cam (*17*). Because x-ray absorption is strongly wavelength-dependent, we integrated this feature into the experimental protocol to trigger the progression from the dioxygen intermediate (**6**) to the activated oxygen species (**7**) by providing the second electron needed for the two-electron redox reaction

Table 1. Sample preparation and data-collection strategy. Crystallization and generation of the ternary P450.cam.O_2 complex. P450cam was expressed and purified as described (*36*). We did not use the orthorhombic crystal form grown from high salt (*37*), but instead we used polyethylene glycol (PEG)–grown monoclinic (and orthorhombic) (*24*) crystals for all experiments performed at cryogenic temperatures. These crystals (0.03 mm by 0.06 mm by 0.3 mm) were grown in sitting drops by mixing 3 to 5 μl of P450 (30 mg/ml) with equal volumes of the reservoir solution [50 mM tris-HCl (pH 7.4), 250 mM KCl, 100 mM DTE, 1 mM camphor, and 27 to 30% PEG 4000]. Time-resolved spectroscopic analysis of microcrystalline slurries was used to obtain the conditions and time windows for generating the ternary P450.cam.O_2 complex (see Fig. 3) before it decays because of autooxidation (*9*). For reduction, crystals were soaked at 2°C in nitrogenated mother liquor containing 50 mM dithionite and 40 mM NaOH until a color change occurred (30 min). Subsequently, the crystals were rinsed in nitrogenated mother liquor for 1 min. Oxygen complexes were made by exposing reduced crystals mounted in a loop with mother liquor containing 20% glycerol to 120-bar oxygen atmosphere for 3 min at 2°C. Then the pressure was released over a period of 30 to 60 s, and the crystals were flash cooled in liquid nitrogen. As described in the text and in this table, three data sets were collected of P450.cam.O_2 crystals kept at cryogenic temperature with an Oxford cryostream. After collection of the first data set (s1) with short-wavelength x-rays, the crystals were exposed to long-wavelength x-rays for about 3 hours, and then the second data set (s2) was collected. The third data set (s3) was collected after briefly thawing the crystals.

Strategy	First data set, s1	X-ray irradiation	Second data set, s2	Warm up	Third data set, s3
What for	O_2 complex	Reduction	Intermediate	Product formation	Product: 5-*exo*-hydroxy-camphor
Why		$[e^-] \sim \exp(\lambda^3]$		$T \gg T_{glass}$ transition	
Wavelength	0.91 Å	1.5 Å	0.91 Å		0.91 Å
Temperature	88 K	96 K	100 K	293 K	100 K
Time		3 hours		≈30 s	

Table 2. Data statistics. Diffraction data were collected at the National Synchrotron Light Source [beamlines X12C (1k x 1k Brandeis charge-coupled device detector) and X8C (MAR Research imaging plate detector)] and at the European Molecular Biology Laboratory c/o Deutsches Elektron-Synchrotron [beamline BW7B (MAR345 detector)]. The XDS program package (*38*) was used for data reduction.

Complex (name)	Temp. (K)	X-ray source λ (Å)	$P2_1$ cell: *a*, *b*, *c* (Å); β, (°)	Resol. (Å)	No. of reflections, overall/unique	Completeness*	$I/\sigma(I)$*	R_{sym}*†
Ferric	100	BW7B, 0.8443	67.4,62.7,95.6 90.6	1.6	242,005/101,044	96.1/95.4	9.4/2.4	6.4/22.7
Reduced	100	X8C, 0.91	67.8,62.8,95.5 90.6	1.9	234,827/61,973	97.6/91.8	11.6/2.7	8.7/34.3
s1	88	X12C, 0.91	67.0,61.8,94.7 90.2	1.8	217,362/69,368	96.6/85.0	9.5/2.2	9.2/38.8
s2	96	X12C, 0.91	66.9,61.7,94.6 90.3	1.9	188,793/60,176	98.8/99.1	9.0/2.9	8.3/23.9
s3	100	X12C, 0.91	67.1,61.9,94.3 90.4	2.3	74,075/58,697	91.2/85.3	6.9/2.4	12.0/31.7

*Completeness, $I/\sigma(I)$, and R_{sym} are given for all data and for the highest resolution shell: ferric, 1.6 to 1.7 Å; reduced, s2, and s3: 2.0 to 1.9 Å; and s1: 1.8 to 1.9 Å. †$R_{sym} = \Sigma|I - \langle I\rangle|/\Sigma I$, where I is the measured intensity and $\langle I\rangle$ is the average of equivalent reflections.

of P450 using the x-ray beam itself.

Thus, after formation of the ferrous enzyme-substrate complex (**5**) by diffusion of dithionite and conversion to the dioxy intermediate (**6**) by exposure to high partial pressure of O_2, three x-ray data sets (s1, s2, and s3) were collected from P450.cam.O_2 crystals frozen in liquid nitrogen and kept at 88 to 100 K during data collection. The first (s1) was collected with short-wavelength x-rays to minimize reduction, thereby keeping the P450.cam.O_2 concentration as high as possible. (It is this consideration that prohibits our use of the Laue method: The white radiation would reduce the P450.cam.O_2 complex while we were trying to observe it.) The second data set (s2) was collected after illuminating the same crystal for 3 hours with long-wavelength x-rays to produce a larger number of hydrated electrons, thereby driving the reaction from the dioxygen species (**5**) toward the reduced, activated oxygen intermediate (**6**). The third (s3) was collected after thawing and refreezing this crystal. This final data set should—and indeed does—correspond to the product complex (**7**). Specific details for each experiment are given in Tables 1 to 3 and the figure legends. All structures were determined by molecular replacement with the known structure of the oxidized camphor.P450cam complex (*4*) as a probe and were refined as described (Tables 1 to 3).

The starting point: Structure of the ferric P450-camphor complex (2). Apart from slight changes in the positions of some surface loops and the presence of a bound tris molecule, the overall structure of the Fe^{III}-P450.cam complex (**2**) in the monoclinic form is very similar to that determined by Poulos and co-workers [Protein Data Bank (PDB) code 2CPP] using an orthorhombic crystal form (*4*). The heme group is covalently attached through its iron to the thiolate sulfur of Cys^{357}. The heme is ruffled and the five-coordinate iron atom is out of the porphyrin plane by 0.3 Å. Camphor is oriented in the distal heme pocket by a single hydrogen bond (2.9 Å) between its carbonyl oxygen atom and the side-chain hydroxyl of Tyr^{96}. The Thr^{101} side chain is rotated compared with 2CPP and forms a hydrogen bond (2.7 Å) to the carboxylate of the propionic acid of the D pyrrole. The hydrogen bond between the hydroxyl group of Tyr^{96} and the carbonyl oxygen of camphor shortened to 2.5 Å (2.9 Å in 2CPP), resulting in a small movement of camphor away from the sixth ligand position. No acidic or basic groups are positioned near the C5 of camphor or the vacant sixth coordination position of iron, nor are ordered water molecules observed near this position.

Addition of the first electron: Structure of the ferrous P450-camphor complex (5). Single electron reduction of Fe^{III}-P450.cam (**2**) to the Fe^{II} form (**5**) is the first step in the process of oxygen activation. The requisite electron was supplied chemically by dithionite, followed by freeze-quenching to stabilize the reduced complex, thus preventing autooxidation to the inactive ferric form (Fig. 1). As predicted from spectroscopic studies (*18*), the structures of the reduced (**5**; Fig. 2A) and oxidized (**2**) forms are very similar. No change in the salt link between Arg^{112}, His^{355}, and the heme 6-propionic group is observed (*19*). The bond length between the iron and the axial thiolate ligand refined to 2.2 Å. However, the resolution of these crystal structures prevents a precise determination of changes in its length (estimated distance error ± 0.2 Å). Again, no ordered water molecules are found near the vacant sixth position.

Binding of molecular oxygen: Structure of the ternary P450.cam.O_2 complex (6). Diffusion of molecular oxygen into the reduced enzyme crystals produced the dioxygen intermediate as indicated spectroscopically (Fig. 3). The structure of this unstable ternary P450.cam.O_2 complex [(**6**); Fig. 2B; Tables 1 to 3] was determined with short-wavelength x-rays to minimize x-ray radiolysis. Diatomic oxygen is bound end-on (η^1) to the heme iron (Table 4) with the distal oxygen atom pointing toward Thr^{252}. Because O_2 binds more bent than CO (Table 4), the sterically induced displacement of camphor upon ligand binding is smaller for O_2 than for CO (*6*); nevertheless, some displacement is observed, providing additional evidence for the

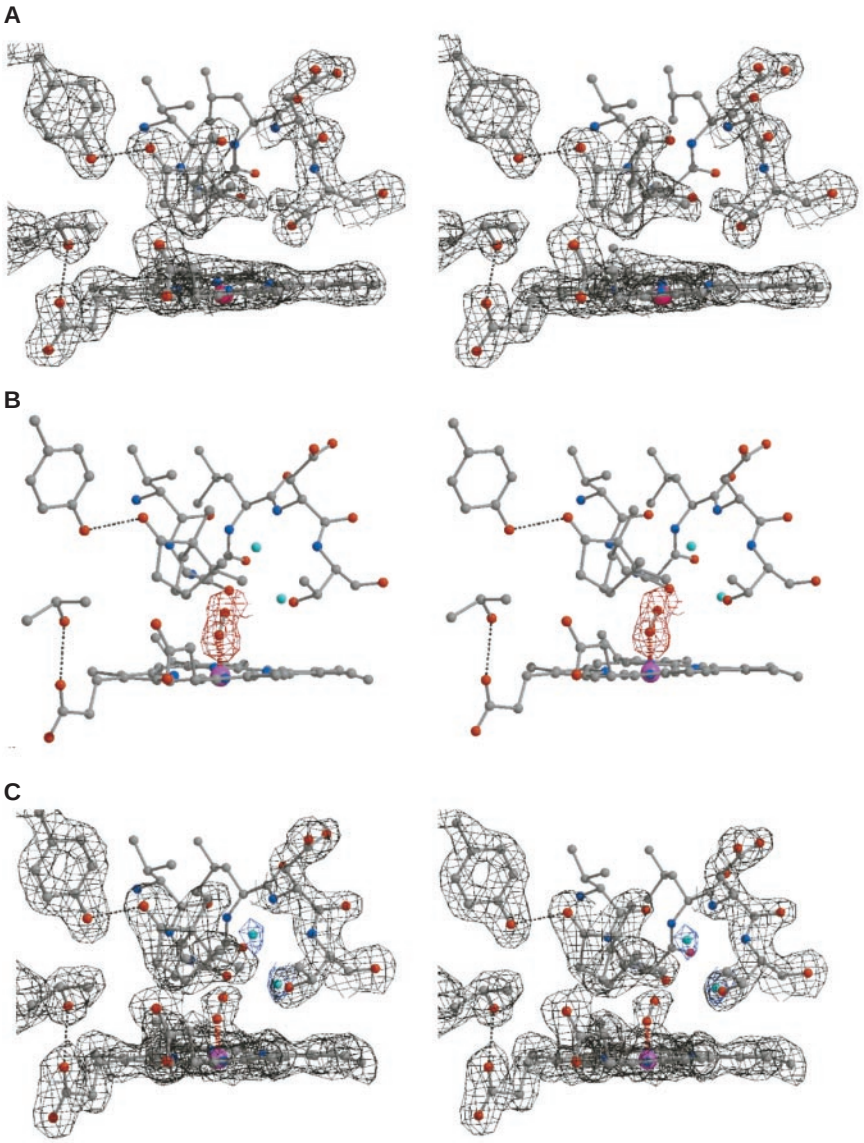

Fig. 2. Stereoviews of electron densities of the different P450 complexes. Map coefficients and contour level are given in parentheses. (**A**) Reduced form (**5**) (σ_A weighted $2F_{obs} - F_{calc}$, 1.3σ). (**B**) Dioxygen complex (**6**) (simulated annealing omitting the O_2 coordinates, $F_{obs} - F_{calc}$, 3σ). (**C**) Final model of P450.cam.O_2; the density for WAT901 and WAT902 is blue (σ_A weighted $2F_{obs} - F_{calc}$, 1.3σ). See text for discussion. The iron is shown as a purple sphere in this and subsequent figures. Figures were generated with Bobscript (*34*) and Raster 3D (*35*).

presence of a diatomic sixth iron ligand. Camphor is within van der Waals contact of this ligand (Fig. 2C). The iron is slightly above the plane of the porphyrin nitrogens and the heme becomes flatter. The bond distance between the heme iron and oxygen is 1.8 Å (Table 4), in agreement with extended x-ray absorption fine structure (EXAFS) and other spectroscopic data (*20*); the distance between the iron and the axial thiolate refined to 2.3 Å.

Water structure in the dioxygen complex. The most obvious changes in the active site upon oxygen binding are the presence of a new, ordered water molecule (WAT901) close to both the dioxygen ligand and the hydroxyl group of Thr^{252} and a new conformation of the backbone atoms of the highly conserved Asp^{251} and Thr^{252} (Fig. 4A) in which the carbonyl oxygen of Asp^{251} has flipped by 90° toward Asn^{255} and the amide nitrogen of Thr^{252} has rotated toward the heme pocket. This movement not only provides hydrogen bonds between the hydroxyl group (3.0 Å) and the amide nitrogen (2.8 Å) of Thr^{252} and WAT901, respectively, but also prevents an unfavorable interaction between the Asp^{251} carbonyl oxygen and the oxygen of WAT901. Both effects, as well as interactions with the carbonyl oxygens of Val^{247} (2.7 Å) and Gly^{248} (2.9 Å), seem to stabilize WAT901 (Fig. 4B). WAT901 sits in the so-called "groove" in the distal I helix (*4*). Widening of the I helix is the result of a hydrogen bond between the hydroxyl group—and not the amide nitrogen as expected for a regular alpha helix—of the highly conserved Thr^{252} and the carbonyl oxygen of Gly^{248}. The "flipped" position of the Asp^{251}-carbonyl oxygen is stabilized by a hydrogen bond to the side-chain amino group of Asn^{255}, which is shifted accordingly. A water molecule (WAT678) bound to it in the ferric complex is not observed. The functional reason for the groove was believed to be the formation of the oxygen-binding niche. However, the P450.cam.O_2 structure indicates another function, the binding of a water molecule.

There is a second water molecule (WAT902) in the P450.cam.O_2 complex (**6**) not present in the ferric, reduced, or carbonmonoxy complexes (Fig. 4A). WAT902 is located next to the hydroxyl group of Thr^{252} (2.1 Å), the carbonyl oxygen of Gly^{248} (2.5 Å), the amide nitrogen of Val^{253} (2.7 Å), WAT687 (2.0 Å), and WAT566 (3.8 Å). WAT901 and WAT902 are 3.4 Å apart. A closed water chain consisting of WAT687, WAT902, WAT566, and WAT523 extends to the side chain of Glu^{366} (Fig. 4B). Other changes near the active site are alternate conformation of the side chain of Thr^{181} and rotated Leu^{244}.

Addition of the second electron: Structure of the intermediate produced by x-ray radiolysis of water (7). We found that irradiation of P450.cam.O_2 (**6**) crystals with long-wavelength x-rays results in changes of the electron density at and around the active site. We interpreted this effect as being due to reduction through radiolytically produced (photo)electrons, possibly derived from solvent or through absorption by the iron, that drive the reaction forward. We hoped to obtain structural information on the (kinetically stabilized) intermediate by collecting data sets of P450.cam.O_2 crystals exposed to long-wavelength x-rays at cryogenic temperature. The most sensitive and least model-biased approach to visualize the x-ray–induced differences is $F_{obs}(s1) - F_{obs}(s2)$ (where F_{obs} and F_{calc} are the observed and calculated structure factors, respectively) electron density maps (Fig. 5A). The biggest feature (maximum 5σ) is the negative difference

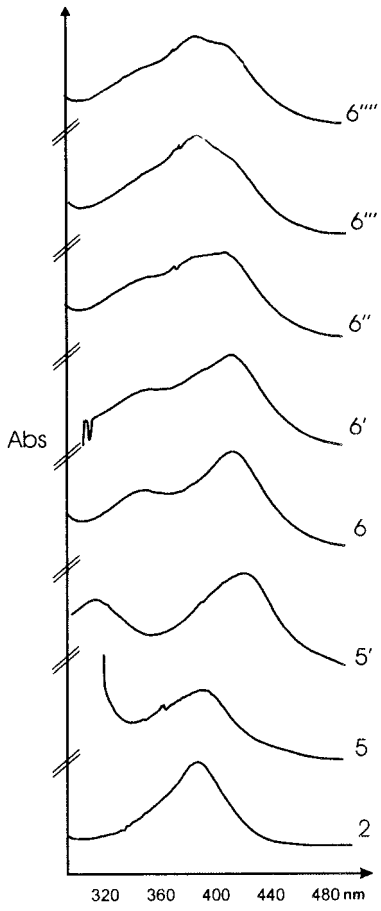

Fig. 3. Spectroscopic analysis of the formation of the reduced and oxygenated substrate complexes of P450cam with microcrystalline slurries mounted in a flow cell and kept at 4°C. The numbers refer to the species in Fig. 1. **2**, ferric P450.camphor complex; **5**, reduced complex with dithionite present; **5′**, while washing with nitrogenated mother liquor; and **6**, addition of oxygenated mother liquor induces formation of the dioxy complex, which slowly decays back to the ferric complex. **6** to **6′′′′** show the spectra obtained 220, 360, 440, 600, and 960 s after oxygen addition, respectively. Abs, absorption.

Table 3. Refinement statistics. The structure of ferric P450.camphor in the monoclinic space group was determined by molecular replacement with the program AMoRe (*39*) with the original structure of the ferric P450.camphor complex as a search model (PDB entry 2CPP). Both molecules in the asymmetric unit were refined independently with XPLOR-3851 (*40*) and CNS (*41*). Refinement included rigid body, simulated annealing, and individual B-factor steps, followed by manual rebuilding with the program "O" (*42*). The sixth ligands were included at the last step of the refinements and covalently attached to the heme iron as was the proximal cysteinate ligand. For the O_2 and oxyferryl complexes of P450cam, the Fe–O and Fe–S distances were weakly restrained to the values determined by EXAFS measurements on P450cam (*20*) and by analysis of model compounds, respectively.

Complex	Resolution (Å)	R_{free}/R_{work}*	rms bond distance (Å)	rms bond angle (°)	No. of water molecules
Ferric	20–1.6	23.7/18.7	0.013	2.46	673
Reduced	19–1.9	25.2/21.1	0.008	1.65	779
s1	15–1.8	24.7/20.3	0.007	1.79	706
s2	20–1.9	25.4/20.2	0.015	1.96	706
s3	20–2.5	27.5/19.4	0.013	2.16	201

*$R_{work} = \Sigma||F_{obs}| - k|F_{calc}||/\Sigma|F_{obs}|$. The same set of 5% randomly chosen reflections was used for calculation of R_{free}.

Table 4. Ligand binding geometry.

Complex	Fifth ligand Fe-SG-Cys^{357} (Å)	Sixth ligand IR* (°)	Bend† (°)	Tilt‡ (°)	Fe-O1§ (Å)	Fe-O2§ (Å)
P450.cam.O_2	≈2.3	43	132	173	1.8	2.9
P450.cam.CO (*9*)	2.4	162	166	5	2.0	3.1

*The infrared angle lies between the normal to the mean heme plane and the O–O or C–O bond, respectively. †The CO/O_2 bend angle is between the iron, the nearer ligand atom, and the farther ligand atom. ‡The tilt angle lies between the line Fe ligand and the normal to the mean heme plane. §O1 denotes the nearer ligand atom and O2 the farther ligand atom.

density at the position of the distal oxygen atom of the O_2 molecule. Because the differences are small, the interpretation and refinement of the corresponding models were not straightforward. The criteria for the—obviously intertwined—validity of the interpretation and the convergence of the refinement were the consistency with the "objective" nonbiased $F_{obs}(s1) - F_{obs}(s2)$ difference peaks, the absence of $F_{obs}(s2) - F_{calc}(s2)$ difference electron density in the refined model, reasonable temperature factors, and chemically sensible distances.

The difference map suggests that O–O bond cleavage has occurred, leaving a single oxygen atom on the heme iron. Simulated annealing omit maps indicate that the conversion is not complete (Fig. 5B). The electron density is too small to accommodate two oxygen atoms, but the elongation of the density could originate from residual O_2. Nevertheless, the electron density (Fig. 5C) is most consistent with an oxy-iron (**7**) species similar to that observed by time-resolved x-ray diffraction studies of the compound I intermediate in cytochrome c peroxidase and catalase (*21*). A single oxygen atom bound to the heme iron at ~1.65 Å distance—substantially closer than the normal Fe–O single-bond distance of 1.8 Å—provided the best fit to the observed electron density. The occupancy of the putative oxyferryl oxygen refined to 60% with a temperature factor of 13 Å^2, the temperature factor of the iron being 14 Å^2 and that of the camphor C5-atom being 18 Å^2. There seems to be a new water molecule WAT903 (occupancy 70%, temperature factor 26 Å^2) close to the oxyferryl oxygen (2.5 Å), the hydroxyl of Thr^{252} (2.5 Å), and the carbonyl of Gly^{248} (2.9 Å), which might be the leaving water molecule produced after O–O bond scission. WAT901 and WAT902 are absent or disordered. The bond distance between the heme iron and the axial thiolate is similar to the one in the oxy complex. Camphor moves by about 0.2 Å toward the heme iron, which is still slightly above the porphyrin plane. This shift of the substrate is consistent with the disappearance of the distal oxygen atom of O_2, which provided a steric barrier. For product formation, C5 must be attacked by the oxygen atom bound to the heme iron, possibly in an oxygen rebound mechanism (*22*), so the movement of camphor makes sense chemically.

There are two concerns about this structure. First, because the rate-limiting step in P450cam is the second electron transfer from putidaredoxin (see Fig. 1), the activated oxygen intermediate (**7**) normally does not accumulate, so why might it be observable here? Perhaps either the restraints on P450 flexibility imposed by the crystal lattice or the unusual source of electrons, or both, combine with the low temperature to change the rate-limiting step. Second, because whatever has occurred is only partially complete, there is likely to be a mixture of species present, which greatly complicates the interpretation. The data show that the predominant species appears to have only a single oxygen atom bound to the iron, but they cannot distinguish between the activated intermediate and, say, a water- or hydroxide-bound heme (met). However, we do not favor an interpretation that assigns the major species to be the met form, because the iron atom is expected to be out of the porphyrin plane on the proximal side in such a complex (*4*), and this structure still has the iron slightly above the porphyrin nitrogens. (The interpretation of the residual electron density below the heme plane in Fig. 5B is unclear; it may indicate anisotropic motion of the iron.) At this point, although the evidence favors the x-ray reduction experiment having produced substantial occupancy of an intermediate on the P450 catalytic pathway, we cannot prove this conclusion and other interpretations remain possible.

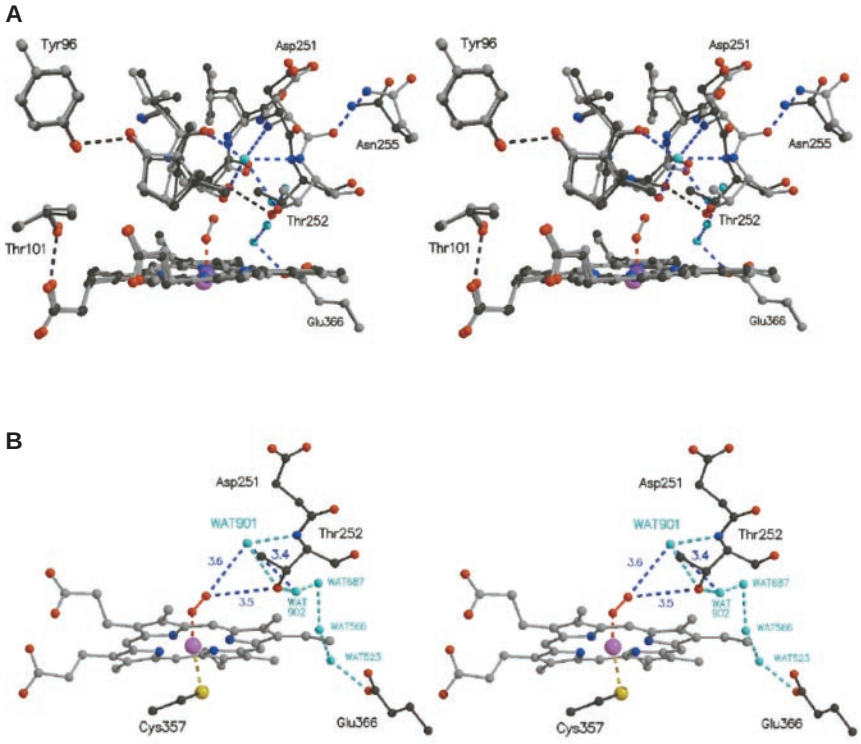

Fig. 4. (**A**) Stereoview of comparison of the camphor complexes of ferrous (dark gray and dark blue water molecules) and ferrous dioxygen-bound (light gray and cyan water molecules) P450. Upon oxygen binding, camphor is displaced, two new water molecules bind, the backbone carbonyl group of Asp^{251} flips, and the backbone amide of Thr^{252} rotates as does its side chain. (**B**) The interactions of the two new water molecules and the water chain extending from the first new water molecule to Glu^{366}. Figures were generated with Bobscript (*34*) and Raster 3D (*35*).

Formation of product: Structure of the complex obtained after warming the radiolytically treated crystals (4). To check if the intermediates we observed are productive, we thawed the radiolytically treated crystals for about 30 s and collected a third data set (s3) (Tables 1 to 3). Thawing and refreezing are accompanied by nonisomorphism, so the structure was determined by molecular replacement. This experiment was repeated with several crystals because the procedure produces disorder. In general, all of the structures show electron density extending from the camphor C5 toward the heme iron, which is still in the porphyrin plane, and are thus consistent with the product complex, 5-*exo*-hydroxycamphor (**4**). These structures are similar to that determined by Poulos and co-workers from co-crystals of P450cam with 5-*exo*-hydroxycamphor (*23*). This agreement includes a change in the position of the Asp^{251} carbonyl, which has flipped back to the original position observed in ferric P450.cam. We confirmed chemically the x-ray–induced generation of 5-*exo*-hydroxycamphor from frozen P450.cam.O_2 solutions using gas chromatography (*24*).

The P450 reaction has an alternate chemical route than two-electron reduction and O_2 binding. This is the peroxide shunt, from the Fe^{III} camphor complex (**2**) to the activated oxygen intermediate (**7**) (Fig. 1). Peroxide can be generated by x-ray radiolysis of water, so we cannot exclude that at least some of the product we observe arises through this route.

The catalytic pathway of P450cam at atomic resolution: Implications for the mechanism. There is evidence to suggest that these structures represent productive intermediates on the catalytic pathway of

P450cam, although we cannot prove this chemically. First, in those structures where we expect a sixth ligand to the heme iron, the iron is observed to be in or slightly above the porphyrin plane, as required. Second, the camphor molecule is observed to move from intermediate to intermediate in a manner consistent with both the demands of catalysis and the steric effects expected for productive complexes. Third, the structures are in good agreement with geometries deduced from spectroscopic data for model systems and for P450s themselves. Fourth, the structures explain the previously puzzling behavior of active site mutants such as $Thr^{252} \rightarrow$ Ala (T252A) or $Asp^{251} \rightarrow$ Asn (D251N) (*25*–*27*). Finally, warming crystals of the putative activated oxygen intermediate produces the correct stereochemical product in situ. Nevertheless, we cannot exclude the possibility that the structures we have determined are artifacts of the experimental conditions or of the packing of P450cam into a crystal lattice. However, if we assume that these structures do represent catalytically competent intermediates, they provide a picture of the P450 reaction pathway in unprecedented detail.

Compared with many other enzymes, P450cam is a relatively rigid catalyst. Conformational changes are restricted to local backbone flips and side-chain reorientations, none of which bring chemically reactive side-chain groups into contact with either the substrate or the bound oxygen. We do not observe any ordered water molecules that are common to all the intermediates. This exclusion may minimize the futile production of hydrogen peroxide from molecular oxygen, a process termed uncoupling (*28*).

Initially (Fig. 1), in the ferric camphor complex (**2**), the heme is ruffled and the five-coordinate iron is 0.3 Å out of plane. This geometry does not change substantially upon addition of the first electron (**5**; Fig. 2A). When molecular oxygen binds (**6**), the heme flattens somewhat and the iron moves to slightly above the plane of the porphyrin nitrogens (Fig. 2, B and C). Small but important conformational changes occur in the protein backbone and side chains in the active site region, leading to the formation of a proton shuttle (Fig. 4B). Oxygen is bound in a bent end-on fashion in a position stabilized by a newly ordered water molecule and by the side-chain hydroxyl of Thr^{252}. Binding of the bulky dioxygen molecule causes camphor to move away from the heme. Addition of the second electron causes cleavage of the O–O bond and produces what may be an oxyferryl species (**7**), with a rather planar heme having the iron slightly above the plane and a short iron-to-oxygen distance suggestive of an Fe=O bond (Fig. 5C). The oxidation state of iron in this species and the electronic state of the heme cannot be determined from these structures. Loss of the terminal oxygen atom partially relieves the steric constraint on the camphor position, allowing the substrate to move back toward the heme; the C5 atom of camphor is then positioned 3.1 Å from the iron-bound oxygen atom, a distance appropriate for (possibly) an oxygen rebound mechanism that produces the 5-OH–camphor product.

Mechanism of oxygen activation: The proton shuttle. Proton transfer is required for cleavage of the iron-bound dioxygen. Proton delivery pathways have been proposed for P450cam involving either two highly conserved residues, Thr^{252} and Asp^{251} (*25*–*27*), or a water chain and the highly conserved Glu^{366} (*29*). Replacement of Asp^{251} by Asn results in a decrease of the catalytic rate by two orders of magnitude with very little uncoupling. On the basis of crystallographic and kinetic isotope studies on the wild-type and D251N mutant of P450cam, Sligar and co-workers proposed a proton shuttle (*25*, *30*) involving two water molecules in the active site. Asp^{251} was implicated in a protein-solvent hydrogen-bonding network delivering protons to the iron-bound dioxygen [Fig. 6 (*25*)]. Replacement of Asp^{251} by Asn would thus disrupt the proton shuttle required for O–O bond cleavage. This proposal is supported by the crystal structures presented here. However, according to the structural data, Asp^{251} seems not to function as a "carboxylate switch" between solvent accessible

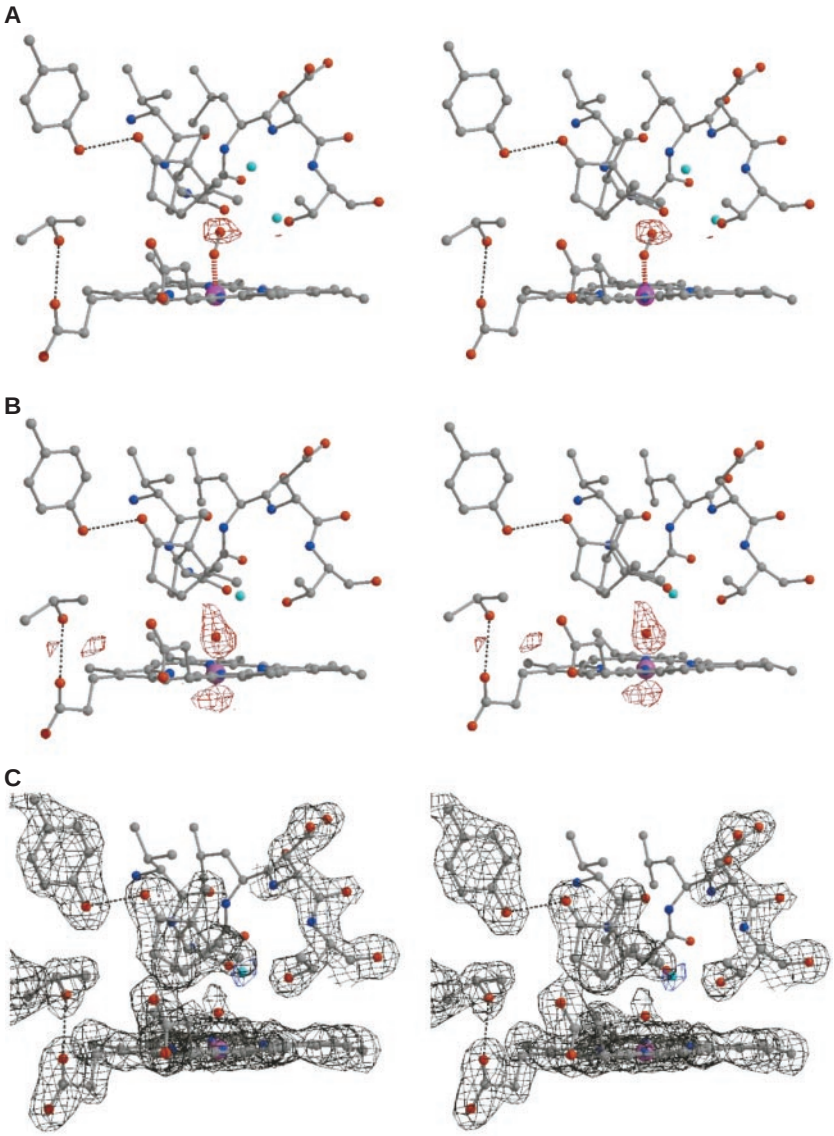

Fig. 5. Stereoviews of electron densities of the different P450 complexes. Map coefficients and contour level are given in parentheses. (**A**) Difference density between data sets s1 and s2 (before and after irradiation with long-wavelength x-rays, respectively) [F_{obs}(s1) − F_{obs}(s2) map, contoured at 3.6σ; the maximum feature is 4.5σ]. (**B**) Data set s2 (simulated annealing map of the final model omitting the oxygen coordinate, $F_{obs} - F_{calc}$, 3σ). (**C**) Final model of the data set s2 interpreted as an oxyferryl (**7**), with WAT903 having blue electron density (σ_A weighted $2F_{obs} - F_{calc}$, 1.3σ). See text for discussion. Figures were generated with Bobscript (*34*) and Raster 3D (*35*).

residues and catalytic water molecules (*25*), but rather as a "carbonyl switch" that stabilizes WAT901. In the ferric and ferrous forms of wild-type P450cam, there are no strong interactions between Asp^{251} and Asn^{255} (Fig. 4A), allowing the carbonyl oxygen of Asp^{251} to flip so as to interact with the amide and amino groups of Asn^{255} upon dioxygen binding (Fig. 4A). This flip is accompanied by rotation of the amide nitrogen of Thr^{252} toward the active site, thereby providing an additional hydrogen bond that stabilizes WAT901.

Replacement of Thr^{252} leads to a large fraction of uncoupling. However, high activity is retained in the $Thr^{252} \rightarrow$ Ser (T252S) mutant and in an artificial mutant that has a methoxy group in place of the hydroxyl group (*31*). Therefore, it was concluded that the role of Thr^{252} in the reaction mechanism is to provide a hydrogen bond. This is confirmed by the structures presented here: Thr^{252} is in hydrogen-bonding distance to the bound dioxygen and to WAT901, a water molecule seen only in the P450.cam.O_2 complex (**6**; Fig. 2C). In the P450(T252A).cam.Fe^{III} complex (*32*) (PDB entry 2CP4), a similar "flipped" conformation of Asp^{251} and Thr^{252} has been observed. In this case, the carbonyl of Asp^{251} rotated by about 120° and is stabilized by an interaction with the main chain amide nitrogen of Asn^{255}. In addition, there is a new water molecule (WAT720) in the mutant that is in hydrogen-bonding distance to the carbonyl oxygen of Gly^{248}. $WAT720_{2CP4}$ binds roughly 1 Å from the position of WAT901 and is located farther away from the groove, perhaps because of a lack of stabilization by the hydroxyl group of Thr^{252}. The oxygen-independent binding and mispositioning of the water molecule in the T252A mutant may be the cause for uncoupling.

There are two water molecules unique for the P450.cam.O_2 complex (**6**; Fig. 2C) that are not observed in the possible P450.cam. oxyferryl structure (**7**; Fig. 5C). Therefore, we interpret them as part of the proton delivery pathway. As described, WAT901 is stabilized indirectly by Asp^{251}, whereas WAT902 is part of a water chain that extends from Thr^{252} to the highly conserved Glu^{366}. Mutation of Glu^{366} to methionine shows little influence on activity (*26*), implying that it does not play a major role in catalysis. On the basis of the structure of the ferric complex of camphor with the T252A mutant (*32*) and on the structures presented here, we speculate that the role of Glu^{366} might be to "anchor" the water chain.

Both WAT687 and the interaction between the hydroxyl group of Thr^{252} and the carbonyl group of Gly^{248} help to stabilize the distal helix in an energetically strained conformation, which seems to be essential to catalysis and to prevent uncoupling. Raag *et al.* (*32*) suggested—as confirmed in the structures presented here—that O_2 binding could initiate a distal I helix rearrangement, thereby promoting binding of a water molecule used in the proton delivery path. (Indeed, both new water molecules WAT901 and WAT902 could not bind to the ferric complex, if only for steric reasons.) As required for this proton delivery mechanism, the side chain of Thr^{252} rotates to interact with both the bound dioxygen molecule and the new water molecules WAT901 and WAT902, which could be the ones required to donate protons for catalysis, as predicted from proton inventory experiments (*25*).

The structures presented here should provide valuable reference points for modeling this reaction, either computationally or by the design and synthesis of model compounds. Because some of the most important reactions in drug metabolism and in the chemical industry involve hydroxylation of unactivated carbon compounds, understanding the P450 reaction has important practical consequences.

Note added in proof: Newcomb *et al*. (*33*) have obtained evidence for the existence of two electrophilic oxidants in the natural course of P450 oxidation reactions, a hydroperoxo-iron species as well as the iron-oxo species. Partial occupancy of a hydroperoxo-iron species could be responsible for the residual electron density seen in the structure of the putative activated oxygen intermediate, and for elongated electron density observed on the iron atom in the second of the two molecules in the asymmetric unit.

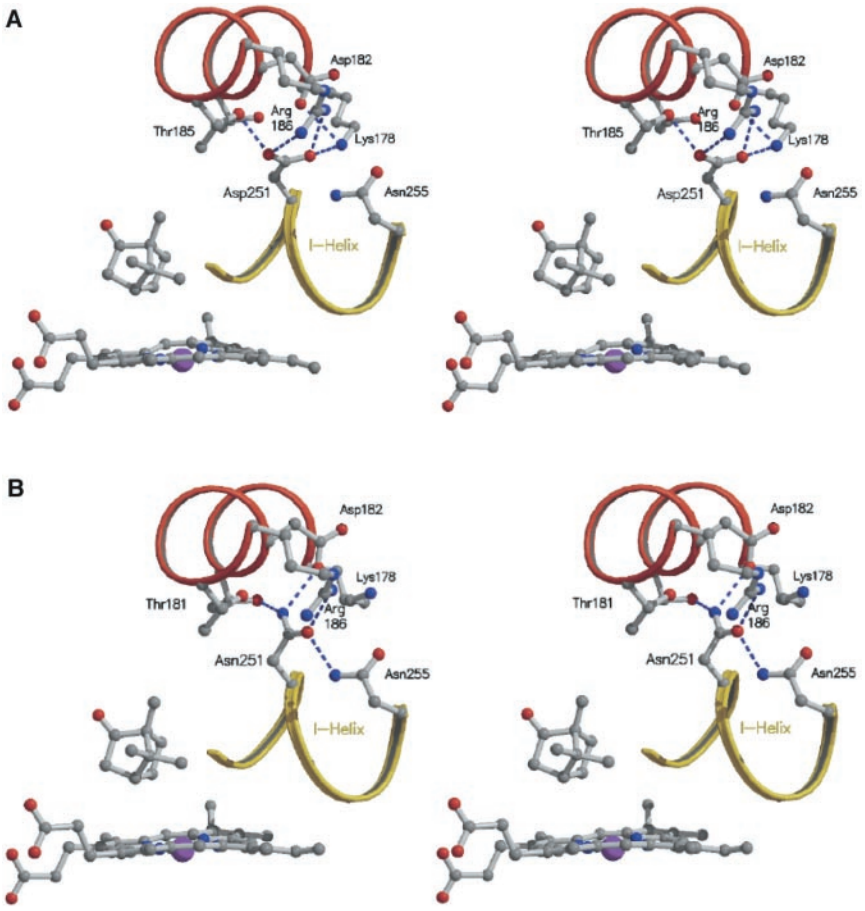

Fig. 6. Stereoviews of comparison of the structures of the ferric camphor complex of wild-type P450 (**A**) and the D251N mutant (PDB entry 6CP4) (**B**). As described in the text, flipping of the Asp^{251}-Thr^{252} backbone, required for stabilization of a presumably catalytic water molecule, is energetically supported by a new hydrogen bond between the carbonyl oxygen of Asp^{251} and the side-chain amide of Asn^{255}. However, in the mutant enzyme, the latter group is involved in a hydrogen bond with the side-chain carbonyl of the mutated residue Asn^{251}. We predict that this reduces the stabilization of the water molecule and thus causes the reduced affinity. Figures were generated with Bobscript (*34*) and Raster 3D (*35*).

References and Notes

1. For a comprehensive review of all aspects of P450, see P. R. Ortiz de Montellano, Ed., *Cytochrome P450: Structure, Mechanism and Biochemistry* (Plenum, New York, ed. 2, 1995).
2. F. P. Guengerich, *J. Biol. Chem.* **266**, 10019 (1991); T. D. Porter and M. J. Coon, *J. Biol. Chem.* **266**, 13469 (1991); J. H. Capdevila, J. R. Falck, R. W. Estabrook, *FASEB J.* **6**, 731 (1992); M. Kubota *et al.*, *J. Biochem.* **110**, 232 (1991).
3. J. Hedegaard and I. C. Gunsalus, *J. Biol. Chem.* **240**, 4038 (1965); C. A. Tyson, J. D. Lipscomb, I. C. Gunsalus, *J. Biol. Chem.* **247**, 5777 (1972); S. G. Sligar and I. C. Gunsalus, *Proc. Natl. Acad. Sci. U.S.A.* **73**, 1078 (1976); E. J. Mueller, P. J. Loida, S. G. Sligar, in *Cyto-*

chrome P450: Structure, Mechanism and Biochemistry, P. R. Ortiz de Montellano, Ed. (Plenum, New York, ed. 2, 1995), pp. 83–124.
4. T. L. Poulos *et al.*, *J. Biol. Chem.* **260**, 16122 (1985); T. L. Poulos *et al.*, *Biochemistry* **25**, 5314 (1986); T. L. Poulos and R. Raag, *FASEB J.* **6**, 674 (1992); H. Li *et al.*, *J. Am. Chem. Soc.* **117**, 6297 (1995). Molecular replacement with the coordinates of oxidized P450cam complexed with camphor (PDB code 2CPP) as search model was used to determine the ferric P450.cam structure in a monoclinic crystal form that contains two molecules per asymmetric unit with an intermolecular K^+ ion binding site. The electron densities of the active sites of the two molecules in the asymmetric unit are not the same, but in different crystals of the same complex, corresponding molecules have similar electron densities, suggesting that the crystal lattice contacts influence the dynamics of the molecules differently. Indeed, the crystallographic environments of the two molecules differ, especially in the vicinity of the intramolecular K^+ binding site, which is connected through Tyr^{96} directly to the camphor binding site. In one molecule, this K^+ site is close to a neighboring molecule in the lattice. In general, for the experiments reported here, similar electron density features are seen in molecules 1 and 2, but mixtures seem to be present in molecule 2 that could not be modeled satisfactorily. It is possible that the two molecules represent slightly different stages of the reaction or different mixtures of species.
5. R. Raag and T. L. Poulos, *Biochemistry* **28**, 7585 (1989).
6. There are many examples; one is the difference between oxy- and carbonmonoxy-myoglobin. See the lively discussion in S. Borman, *Chem. Eng. News* **77**, 31 (1999).
7. The number of model compounds that have been synthesized and characterized is too great to permit referencing even a representative sample. For a recent review, see J. T. Groves and Y. Han, in *Cytochrome P450: Structure, Mechanism and Biochemistry*, P. R. Ortiz de Montellano, Ed. (Plenum, New York, ed. 2, 1995), pp. 3–48.
8. R. E. White and M. J. Coon, *Annu. Rev. Biochem.* **49**, 315 (1980); V. P. Miller *et al.*, *J. Biol. Chem.* **267**, 8936 (1992); W. R. Patterson *et al.*, *Biochemistry* **34**, 4342 (1995).
9. S. G. Sligar, J. D. Lipscomb, P. G. Debrunner, I. C. Gunsalus, *Biochem. Biophys. Res. Commun.* **61**, 290 (1974); C. B. Brewer and J. A. Peterson, *Arch. Biochem. Biophys.* **249**, 515 (1986).
10. B. L. Stoddard, *Pharmacol. Ther.* **70**, 215 (1996).
11. I. Schlichting and R. S. Goody, *Methods Enzymol.* **277**, 467 (1997).
12. D. Ringe *et al.*, *Philos. Trans. R. Soc. London Ser. A* **340**, 243 (1992).
13. J. Hajdu and I. Anderson, *Annu. Rev. Biophys. Biomol. Struct.* **22**, 467 (1993).
14. G. A. Petsko, *Philos. Trans. R. Soc. London Ser. A Math. Phys. Sci.* **340**, 323 (1992).
15. J. D. Lipscomb, S. G. Sligar, M. J. Namtvedt, I. C. Gunsalus, *J. Biol. Chem.* **251**, 1116 (1976).
16. B. Chance, P. Angiolillo, E. K. Yang, L. Powers, *FEBS Lett.* **112**, 178 (1980); J. G. De Witt *et al.*, *J. Am. Chem. Soc.* **113**, 9219 (1991); R. Watanabe, N. Usami, K. Kobayashi, *Int. J. Radiat. Biol.* **68**, 113 (1995); Y. Lindquist, W. J. Huang, G. Schneider, J. Shanklin, *EMBO J.* **15**, 4081 (1996); M. Erikson, A. Jordan, H. Eklund, *Biochemistry* **37**, 13349 (1998); E. R. Stadtman, *Annu. Rev. Biochem.* **62**, 797 (1993).
17. K. Kobayashi *et al.*, *Biochim. Biophys. Acta* **1037**, 297 (1990); R. Davydov *et al.*, *FEBS Lett.* **295**, 113 (1991).
18. M. Sharrock *et al.*, *Biochim. Biophys. Acta* **420**, 8 (1976); M. J. Honeychurch, A. O. Hill, L. L. Wong, *FEBS Lett.* **451**, 351 (1999).
19. J. Contzen and C. Jung, *Biochemistry* **38**, 16253 (1999).
20. J. H. Dawson *et al.*, *J. Am. Chem. Soc.* **108**, 8114 (1986); D. Harris, G. Loew, L. Waskell, *J. Am. Chem. Soc.* **120**, 4308 (1998).
21. V. Fülöp *et al.*, *Structure* **2**, 201 (1994); S. L. Edwards, H. X. Nguyen, R. C. Hamlin, J. Kraut, *Biochemistry* **26**, 1503 (1987); P. Gouet *et al.*, *Nature Struct. Biol.* **3**, 951 (1996).
22. J. T. Groves and G. A. McClusky, *Biochem. Biophys. Res. Commun.* **81**, 154 (1978); J. T. Groves and D. V. Subramanian, *J. Am. Chem. Soc.* **106**, 2177 (1984).
23. H. Li, S. Narasimhulu, L. M. Havran, J. D. Winkler, T. L. Poulos, *J. Am. Chem. Soc.* **117**, 6297 (1995).
24. I. Schlichting *et al.*, data not shown.
25. M. Vidakovic, S. G. Sligar, H. Li, T. L. Poulos, *Biochemistry* **37**, 9211 (1998).
26. H. Shimada, R. Makino, M. Unno, T. Horiuchi, Y. Ishimura, in *Cytochrome P450. 8th International Conference*, M. C. Lechner and J. Libbey, Eds. (Eurotext, Paris, 1994), pp. 299–306.
27. N. C. Gerber and S. G. Sligar, *J. Biol. Chem.* **269**, 4260 (1994); J. Aikens and S. G. Sligar, *J. Am. Chem. Soc.* **116**, 1143 (1994); S. A. Martinis, W. M. Atkins, P. S. Stayton, S. G. Sligar, *J. Am. Chem. Soc.* **111**, 9252 (1989).
28. P. J. Loida and S. G. Sligar, *Biochemistry* **32**, 11530 (1993).
29. D. L. Harris and G. H. Loew, *J. Am. Chem. Soc.* **118**, 6377 (1996).
30. D. E. Benson, K. S. Suslick, S. G. Sligar, *Biochemistry* **36**, 5104 (1997).
31. Y. Kimata, S. Tsukada, T. Iwamoto, K. Harii, *Biochem. Biophys. Res. Commun.* **208**, 96 (1995).
32. R. Raag, S. A. Martinis, S. G. Sligar, T. L. Poulos, *Biochemistry* **30**, 11420 (1991).
33. M. Newcomb *et al.*, *J. Am. Chem. Soc.* in press.
34. R. M. Esnouf, *J. Mol. Graphics* **15**, 133 (1997).
35. E. A. Meritt and M. E. P. Murphy, *Acta Crystallogr. Sect. D* **50**, 869 (1994).
36. N. C. Gerber and S. G. Sligar, *J. Am. Chem. Soc.* **114**, 8742 (1992).
37. T. L. Poulos, M. Perez, G. C. Wagner, *J. Biol. Chem.* **257**, 10427 (1982).
38. W. Kabsch, *J. Appl. Crystallogr.* **26**, 795 (1993).
39. J. Navaza, *Acta Crystallogr. Sect. A* **50**, 157 (1994).
40. A. T. Brünger, *X-PLOR: A System for Crystallography and NMR, version 3.1* (Yale Univ. Press, New Haven, CT, 1992).
41. A. T. Brünger *et al.*, *Acta Crystallogr. Sect. D* **54**, 905 (1998).
42. T. A. Jones, S. Cowan, J. Y. Zou, M. Kjeldgaard, *Acta Crystallogr. Sect. A* **47**, 110 (1991).
43. The literature of cytochrome P450 is so vast, and so many people have made important contributions, that it is impossible in the space allowed to give even a representative set of references. We have tried to cite review articles whenever possible to provide links to the original papers. We apologize to those we have been unable to include. We gratefully acknowledge G. Holtermann for designing the pressure cell; M. Davies, N. C. Gerber, E. J. Mueller, and M. Vidakovic for supplying us with protein; C. Jung, G. Rosenbaum, and K. Scheffzek for discussions; and R. S. Goody, K. C. Holmes, and W. Kabsch for continuous support and encouragement. P. Ortiz de Montellano and J. A. Peterson provided useful advice. The referees made a number of very helpful suggestions that greatly improved the manuscript. We thank the Alexander von Humboldt Stiftung, the Human Frontiers Science Project, and the Richard und Anne Liese Leyendecker Stiftung for generous support and acknowledge the European Community biotech grant BIO2-CT942060 to I.S., NIH grants GM31756 and GM33775 to S.G.S, and GM26788 to G.A.P. and D.R. Beamline X12C is supported by the U.S. Department of Energy Offices of Health and Environmental Research and of Basic Energy Sciences, NIH, and NSF. The coordinates have been submitted to the PDB: 1d26, 1d24, 1d28, and 1d29 for the ferric, reduced, oxy, and oxyferryl complex, respectively.

22 October 1999; accepted 1 February 2000

Mid-Pleistocene Acheulean-like Stone Technology of the Bose Basin, South China

Hou Yamei,[1] Richard Potts,[2]* Yuan Baoyin,[3] Guo Zhengtang,[3] Alan Deino,[4] Wang Wei,[5] Jennifer Clark,[2] Xie Guangmao,[6] Huang Weiwen[1]

Stone artifacts from the Bose basin, South China, are associated with tektites dated to 803,000 ± 3000 years ago and represent the oldest known large cutting tools (LCTs) in East Asia. Bose toolmaking is compatible with Mode 2 (Acheulean) technologies in Africa in its targeted manufacture and biased spatial distribution of LCTs, large-scale flaking, and high flake scar counts. Acheulean-like tools in the mid-Pleistocene of South China imply that Mode 2 technical advances were manifested in East Asia contemporaneously with handaxe technology in Africa and western Eurasia. Bose lithic technology is associated with a tektite airfall and forest burning.

A boundary between East Asia and western Eurasia/Africa was defined by Movius (*1*, *2*) to mark a geographic separation in early human technology and behavioral competence during most of the Pleistocene. Movius and others (*3*) observed that technologically simple methods of stone flaking persisted in China and Southeast Asia during the period when ovate large cutting tools (LCTs), specifically Acheulean bifacial handaxes and cleavers, characterized western Eurasia and Africa (currently dated at 1.6 to 0.2 million years ago). The boundary, known as the Movius Line, implies that Pleistocene East Asian populations were culturally and possibly genetically isolated (*4*), a situation that was reinforced by stable forest habitat east of the boundary (*2*, *5*). Although the Movius Line has attracted criticism (*6*–*8*), little evidence to contradict it has been presented (*9*, *10*). Analyses of Acheulean technology (*11*, *12*) have concluded that the targeted manufacture of LCTs signifies an important advance in hominin behavior (enhanced planning and technical competence) for which evidence has been lacking in the early stone technology of East Asia.

Here we describe stone tools from the